https://doi.org/10.14669/AM/224717

DEVELOPMENT AND PERFORMANCE EVALUATION OF AN INTELLIGENT MOBILE HYBRID RENEWABLE ENERGY SYSTEM FOR AUTOMOTIVE APPLICATIONS

SEBASTIAN BIAŁASZ[1], MAŁGORZATA SZAFRANIEC[2,3], MARCIN DĘBOWSKI[4], KONRAD PIETRYKOWSKI[5,6], GRZEGORZ PIĄTEK[7]

Abstract

This paper presents the development and comprehensive performance evaluation of an innovative mobile hybrid renewable energy system designed for automotive and off-grid applications. The research addresses a critical gap in the market for portable power generation solutions that combine high energy density, environmental sustainability, and operational flexibility. The trailer-mounted system integrates a 9 kW photovoltaic installation with dual-axis solar tracking, two novel vertical-axis wind turbines (VAWT) with combined 800 W output, and a 9 kWh lithium-ion battery storage system with intelligent energy management. Key innovations developed during this research include a proprietary folding blade VAWT design achieving 31% aerodynamic efficiency, representing a 55% improvement over baseline Savonius rotors while maintaining acoustic emissions below 45 dBA suitable for noise-sensitive environments. The dual-axis tracking system provides 26.3% annual energy gain with only 3.3% parasitic consumption, yielding an exceptional net energy gain ratio of 7.58 that substantially exceeds commercial alternatives. Additionally, nanocellulose-based

1 R&D Center, Albi-Tech Sp. z o.o. Dobrzańskiego 3, 20-262, Lublin, Poland, email: biuro@albi-tech.pl, ORCID: 0009-0006-1560-2954

2 R&D Center, Albi-Tech Sp. z o.o. Dobrzańskiego 3, 20-262, Lublin, Poland, email: biuro@albi-tech.pl

3 Faculty of Civil Engineering and Architecture, Lublin University of Technology, Lublin, Poland, email: malgosiaszafraniec@gmail.com, ORCID: 0000-0002-5862-9456

4 R&D Center, Albi-Tech Sp. z o.o. Dobrzańskiego 3, 20-262, Lublin, Poland, email: marcin.debowski@energolink.pl

5 R&D Center, Albi-Tech Sp. z o.o. Dobrzańskiego 3, 20-262, Lublin, Poland, email: biuro@albi-tech.pl

6 Faculty of Mechanical Engineering, Lublin University of Technology, Lublin, Poland, email: k.pietrykowski@pollub.pl, ORCID: 0000-0001-6497-7572

7 Gewe sp. z o.o., GEWE Sp. z o.o. Lublin, Poland, email: biuro@przyczepka.pl

https://doi.org/10.14669/AM/224717

anti-soiling coatings derived from recycled paper waste reduce dust adhesion by 68.75%, addressing a significant source of efficiency losses in mobile applications.
Wind tunnel testing validated turbine performance across wind speeds from 6 m/s to 14 m/s, while computational fluid dynamics (CFD) analysis confirmed structural stability under 72 km/h crosswind conditions with a safety factor of 2.14 against overturning. Field validation over 12 months demonstrated annual energy production of 10.6 MWh with a power-to-weight ratio of 8.17 W/kg, representing a 73% improvement over the best commercial portable solar systems. The system's unique capability to generate energy during transport at 33% capacity addresses a critical limitation of existing mobile renewable energy solutions.
Results demonstrate significant potential for reducing diesel generator dependency in construction, outdoor events, emergency response, and military applications. The research contributes novel turbine designs, validated tracking algorithms, and sustainable coating technologies applicable to broader renewable energy applications.

Keywords: mobile renewable energy; vertical-axis wind turbine; hybrid power system; off-grid power; automotive trailer; CFD analysis; anti-soiling technology

1. Introduction

1.1. Background and Motivation

The global transition toward sustainable energy systems has created unprecedented demand for portable and mobile power generation solutions. Construction sites, outdoor events, emergency response operations, agricultural applications, and military deployments increasingly require reliable off-grid power without the environmental impact, noise pollution, and logistical complications associated with conventional diesel generators. The transport sector remains one of the largest sources of energy-related CO_2 emissions, releasing nearly 8 Gt of CO_2 in 2022 [1]. Within this sector, diesel-fuelled generators used to supply off-grid and portable power are a particularly carbon- and pollutant-intensive option, underscoring the urgent need for cleaner alternatives that can operate independently of grid infrastructure.

The renewable energy sector has made remarkable progress in stationary applications [2], with solar photovoltaic and wind power costs declining by over 80% in the past decade [3]. However, the mobile and portable renewable energy segment has not experienced comparable advancement. As reviewed in Section 1.2, current mobile solar solutions suffer from several fundamental limitations that restrict their practical utility. First, power-to-weight ratios typically remain below 5 W/kg, meaning that significant trailer capacity must be dedicated to the power generation equipment itself rather than useful payload or equipment. Second, existing systems cannot generate any energy during transport between deployment sites, creating operational dead time that reduces overall system utilization and economic viability.

https://doi.org/10.14669/AM/224717

Wind energy integration in mobile platforms presents even greater challenges. Horizontal-axis wind turbines (HAWT), while efficient in stationary installations, are poorly suited for mobile deployment due to their requirement for consistent wind direction, structural complexity, and significant acoustic emissions. Vertical-axis wind turbines (VAWT) offer potential advantages for mobile applications, including omnidirectional wind acceptance, lower acoustic signatures, and simpler structural requirements [4, 5]. However, conventional VAWT designs such as the Savonius rotor suffer from relatively low aerodynamic efficiency, typically achieving power coefficients (Cp) of only 15–20%, limiting their practical energy contribution [6].

Furthermore, existing mobile renewable energy solutions rarely address the compound efficiency losses caused by environmental factors. Dust accumulation on photovoltaic surfaces can reduce panel output by 20–40% [7] within weeks of deployment in construction or agricultural environments, necessitating frequent manual cleaning that may not be practical in remote locations. The development of effective anti-soiling technologies specifically designed for mobile applications represents an important but largely neglected research area.

The automotive sector provides a particularly compelling application domain for mobile renewable energy systems. The rapid expansion of electric vehicle (EV) fleets has created an urgent demand for flexible charging infrastructure that can be deployed at construction sites, temporary events, highway rest areas, and disaster relief locations where permanent grid-connected charging stations are unavailable or economically impractical. Current mobile EV charging solutions rely predominantly on diesel generators, creating a paradoxical situation where zero-emission vehicles are charged using fossil-fuel-powered equipment. Furthermore, the electrification of construction and agricultural machinery introduces additional demand for mobile high-power renewable charging capability. The development of a trailer-mounted hybrid renewable energy system capable of providing Level 2 AC charging directly addresses this emerging market need while simultaneously reducing the carbon footprint of the transport sector's supporting infrastructure. The intersection of renewable energy engineering, automotive trailer design, and transport electrification represents a multidisciplinary research challenge that has received insufficient attention in the existing literature.

1.2. State of the Art in Mobile Renewable Energy

The current market for mobile renewable energy solutions is dominated by three main product categories: portable solar generators, trailer-mounted solar systems, and hybrid solar-diesel solutions. Portable solar generators, exemplified by products such as the Goal Zero Yeti series and Jackery Explorer systems, offer convenience and ease of deployment but are limited to power outputs below 6 kW and lack the scalability required for commercial

https://doi.org/10.14669/AM/224717

or industrial applications. These systems achieve power-to-weight ratios of approximately 4–5 W/kg and provide no energy generation during transport.

Trailer-mounted solar systems represent the current state-of-the-art for higher-power mobile applications. Companies such as Mobile Solar Power, SunTech Solar, and Renovagen offer systems ranging from 10 kW to 100 kW capacity. However, these systems typically employ fixed-tilt or single-axis tracking, sacrificing 15–25% of potential energy capture compared to dual-axis tracking alternatives. Additionally, deployment times for larger systems can exceed 30 minutes, and the systems require specialized personnel for setup and operation. Wind energy integration in these commercial products is virtually nonexistent due to the engineering challenges involved.

Research literature on mobile renewable energy has focused primarily on vehicle-integrated photovoltaics (VIPV) for electric vehicle range extension and building-integrated photovoltaics (BIPV) for temporary structures. Studies by Araki et al. [8] demonstrated that high-efficiency III-V multijunction cells can provide meaningful range extension for electric vehicles, while Pillai et al. [9] reviewed building-integrated photovoltaics for sustainable construction. However, comprehensive research on integrated mobile hybrid systems combining solar, wind, and storage in an optimized trailer platform remains limited.

Vertical-axis wind turbine research has advanced significantly in recent years, with studies by Lee et al. [4], Hand et al. [10], and Wong et al. [11] demonstrating improved performance through optimized blade profiles, multiple rotor stages, and innovative starting mechanisms. Nevertheless, these advances have not been translated into commercial mobile wind energy products, and specific research on VAWT designs optimized for trailer-mounted applications is notably absent from the literature. To date, no published study has presented a fully integrated mobile platform combining dual-axis tracked photovoltaics, optimized VAWTs, intelligent energy management, and circular-economy-derived anti-soiling coatings in a single road-legal trailer configuration.

A systematic review of the academic literature reveals that existing studies on mobile renewable energy systems have addressed individual subsystems in isolation rather than as integrated platforms. Elahi Gol and Ščasný [12] estimated that sun-tracking produces approximately 20–30% more energy than a comparable fixed structure, with the tracker's levelized cost of energy up to 20% lower than that of a fixed system but did not address the specific constraints of mobile deployment including vibration, rapid repositioning, and parasitic energy minimization. Awasthi et al. [13] provided a comprehensive review of tracking methods but noted the absence of validated tracking data for trailer-mounted configurations. In the wind energy domain, Griffith et al. [5] explored innovative VAWT rotor concepts for offshore applications, while Lee et al. [4] and Wong et al. [11] evaluated performance enhancement strategies for vertical-axis turbines, yet none of these studies considered the unique requirements of mobile deployment including compact folding mechanisms,

https://doi.org/10.14669/AM/224717

low-noise operation in proximity to personnel, and aerodynamic stability during road transport. The anti-soiling research by Uddin [7] quantified dust-related efficiency losses for stationary installations but did not explore coating solutions optimized for the variable environmental conditions encountered by mobile systems operating across diverse deployment sites. The present work addresses these gaps by developing and validating an integrated system architecture that simultaneously advances multiple technology domains while quantifying their combined performance under realistic field conditions.

1.3. Research Objectives and Scope

This research addresses the identified gaps through the development of an intelligent mobile hybrid renewable energy system that combines photovoltaic and wind energy generation with advanced tracking, novel turbine designs, and innovative surface treatments. The system is designed to maximize energy production per unit mass while maintaining practical deployment characteristics suitable for diverse applications including construction sites, outdoor events, emergency response, and military operations.

The primary objectives of this study were organized into four interconnected research areas. First, to develop and validate a novel VAWT design optimized specifically for mobile trailer applications, with emphasis on achieving high aerodynamic efficiency at moderate wind speeds (6–14 m/s), low acoustic emissions suitable for noise-sensitive environments, and a compact folding mechanism for transport. Second, to quantify the energy gains achievable from dual-axis solar tracking in a mobile platform configuration, including detailed analysis of parasitic energy consumption and net energy gain ratios across seasonal variations.

Third, to develop and evaluate nanocellulose-based anti-soiling coatings derived from recycled waste materials for photovoltaic applications, addressing both the practical need for reduced maintenance and the broader sustainability objectives of circular economy principles. Fourth, to assess the aerodynamic stability and overall system performance under realistic operating conditions through computational fluid dynamics simulation and extended field testing.

The scope of this research encompasses the complete development cycle from conceptual design through prototype fabrication, laboratory testing, and field validation. The research was conducted as part of an R&D project in collaboration between Albi-Tech Sp. z o.o., Lublin University of Technology, and GEWE Sp. z o.o., combining academic research capabilities with industrial expertise in trailer manufacturing and renewable energy systems. The range of trailer platform configurations available from GEWE is presented in Figure 1.

https://doi.org/10.14669/AM/224717

Fig. 1. Overview of trailer platform configurations available from GEWE Sp. z o.o. for mobile energy system integration

2. Materials and Methods

2.1. System Architecture and Configuration

The mobile renewable energy system was designed around a standard two-axle automotive trailer platform manufactured by GEWE Sp. z o.o., with gross vehicle weight rating (GVWR) of 3,500 kg and permissible road speed of 100 km/h. As in Figure 2, the trailer platform measures 6.0 m in length, 2.5 m in width, and 0.8 m in deck height, providing a base structure capable of accommodating the photovoltaic array, wind turbines, battery storage, power electronics, and auxiliary systems while maintaining road-legal dimensions and weight distribution.

Fig. 2. CAD model of the mobile hybrid renewable energy system showing trailer platform, dual-axis tracking frame, and integrated wind turbines

https://doi.org/10.14669/AM/224717

The system architecture comprises four integrated subsystems: photovoltaic generation with dual-axis tracking, wind energy conversion with novel VAWT design, energy storage and power conditioning, and intelligent control and monitoring. These subsystems were designed for synergistic operation, with the control system optimizing energy flow between generation sources, storage, and load based on real-time conditions and predictive algorithms.

2.1.1. Photovoltaic Subsystem

The photovoltaic subsystem consists of 24 monocrystalline silicon panels arranged in a 4×6 array configuration, providing a combined peak output of 9 kWp under Standard Test Conditions (STC: 1000 W/m², 25°C cell temperature, AM1.5 spectrum). Individual panels are rated at 375 Wp each with an efficiency of 20.4% and dimensions of 1755 mm × 1038 mm × 35 mm. The panels were selected based on their combination of high efficiency, mechanical durability, and excellent low-light performance, with a temperature coefficient of -0.35%/°C for power output.

The panel array is mounted on an automated dual-axis tracking frame constructed from aluminum extrusion profiles and galvanized steel structural members. The frame design prioritizes both structural integrity during transport and operational conditions, and minimal mass to maximize the system power-to-weight ratio (Figure 3). Total frame mass including drive mechanisms is 185 kg, representing a frame-specific power density of 48.6 W/kg.

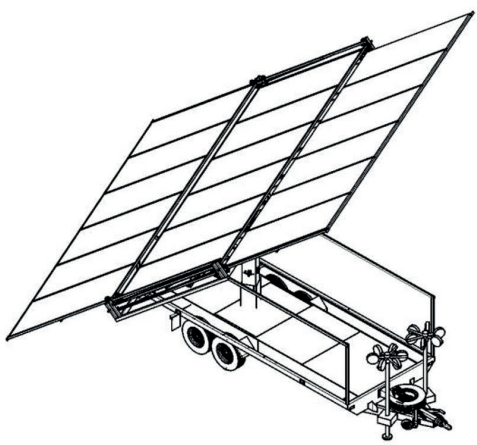

Fig. 3. Technical drawing of the mobile solar trailer showing dual-axis tracking mechanism and panel array configuration

Deployment from transport to operational configuration is achieved within 5 minutes through an electromechanical actuator system. In transport mode, the panel array is folded flat on the trailer deck with the panels oriented face-down to protect the glass surface. Deployment

https://doi.org/10.14669/AM/224717

involves raising the array to vertical orientation on the central support column, then tilting to the appropriate elevation angle while the azimuth drive positions the array toward the sun. The deployment sequence is fully automated and can be initiated from the integrated control panel or remotely via cellular communication.

2.1.2. Wind Energy Subsystem

Wind energy generation is provided by two vertical-axis wind turbines positioned at the forward corners of the trailer. Each turbine is rated at 400 W nominal output at 10 m/s wind speed with a rotor diameter of 1.2 m for the full-scale production units, though testing was conducted on 700 mm diameter prototypes for wind tunnel compatibility. The VAWT configuration was selected for its omnidirectional wind acceptance eliminating the need for yaw control, lower acoustic emissions compared to horizontal-axis designs, and inherent suitability for the turbulent wind conditions encountered in mobile applications where site-specific wind patterns cannot be anticipated.

The turbines incorporate a folding mechanism that allows them to be collapsed to a transport height of approximately 0.4 m, compared to the operational height of 1.8 m. This folding capability is essential for maintaining road-legal transport dimensions and reducing aerodynamic drag during highway transit (Figures 4, 5). The folding mechanism employs a telescoping central shaft with locking collar, allowing a deployment in under 30 seconds per turbine.

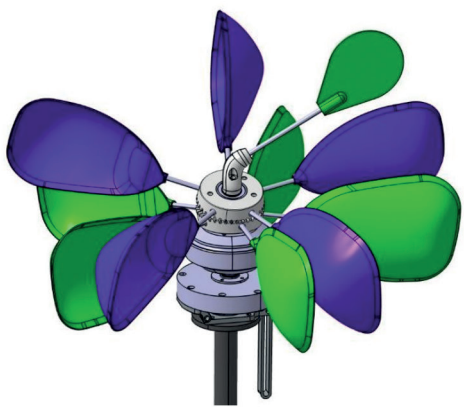

Fig. 4. CAD model of the novel folding blade VAWT design showing articulated blade segments and hub mechanism

https://doi.org/10.14669/AM/224717

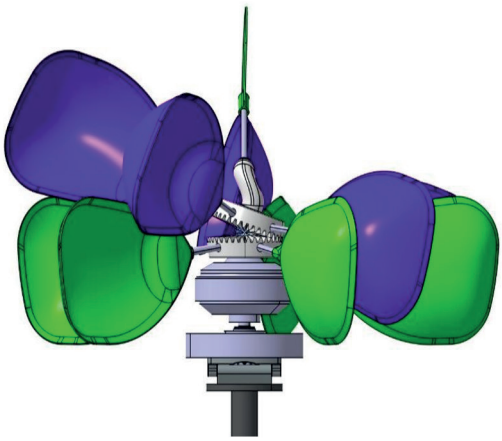

Fig. 5. Alternative view of the folding blade VAWT showing blade orientation during operation

2.1.3. Energy Storage and Power Conditioning

Energy storage is provided by a modular lithium iron phosphate ($LiFePO_4$) battery system with 9 kWh usable capacity, corresponding to approximately 10.8 kWh nominal capacity at 80% depth of discharge. The battery system comprises three 48V, 100 Ah modules connected in parallel, providing redundancy and allowing continued operation if one module requires maintenance. $LiFePO_4$ chemistry was selected for its superior cycle life (>3000 cycles at 80% DoD), thermal stability, and safety characteristics compared to other lithium-ion chemistries.

The battery management system (BMS) incorporates cell-level voltage monitoring, active balancing, and thermal management with liquid cooling capability for high ambient temperature operation. State-of-charge estimation employs a Coulomb counting algorithm with periodic recalibration based on open-circuit voltage measurements during idle periods. The BMS communicates with the central control system via CAN bus, providing real-time data on battery status, available capacity, and recommended charge/discharge limits.

Power conditioning is handled by a 10 kVA hybrid inverter capable of grid-tie, off-grid, and vehicle-to-load operation modes. In off-grid mode, the inverter synthesizes a 230V, 50Hz AC output from the DC bus, with automatic transfer to generator input if available. Grid-tie mode allows export of excess energy to the utility grid when the system is connected, with anti-islanding protection per EN 50549 [14] requirements. The inverter incorporates maximum power point tracking (MPPT) for the photovoltaic array with tracking efficiency exceeding 99.5%.

https://doi.org/10.14669/AM/224717

2.2. Vertical-Axis Wind Turbine Development

The development of an optimized VAWT design for mobile applications constituted a major focus of this research. Three distinct rotor configurations were developed and tested: a baseline Savonius rotor (designated M1), a dual-rotor angular design (M2), and a novel folding blade design (M3). All prototypes shared a 700 mm rotor diameter and 800 mm rotor height to enable direct performance comparison in the wind tunnel test facility.

2.2.1. Rotor Design Configurations

The baseline Savonius rotor (M1) employed a conventional two-blade configuration with semi-cylindrical blade profile and 15% blade overlap ratio. The Savonius design represents the simplest VAWT configuration and provides a well-characterized baseline for performance comparison. Blades were fabricated from 1.5 mm sheet aluminum formed over wooden molds, with end plates to reduce tip losses.

The dual-rotor angular design (M2) utilized two vertically-stacked three-blade rotors with 30° angular offset between the upper and lower rotor stages. This configuration was hypothesized to reduce torque ripple and improve starting characteristics compared to single-stage designs. Each rotor stage employed helical blade twist of 15° over the blade span to distribute aerodynamic loads and further smooth torque output. Blades were fabricated from fiberglass-reinforced polymer using vacuum infusion molding.

The folding blade design (M3) incorporated a novel mechanism wherein articulated blade segments adjust their orientation based on angular position during rotation. Each blade consists of two hinged segments connected by a cam-and-follower mechanism that causes the outer segment to rotate relative to the inner segment as the rotor turns. This variable geometry effectively combines lift and drag forces throughout the rotation cycle, addressing a fundamental limitation of fixed-geometry VAWT designs where one blade is always moving against the wind (Figure 6).

The folding blade mechanism was designed using kinematic synthesis techniques to achieve optimal blade orientation at key angular positions: maximum drag coefficient when the blade is advancing with the wind (0° position), transition to lift-dominated forces in the side positions (90° and 270°), and minimum drag when the blade is retreating against the wind (180° position). The mechanism adds approximately 15% to rotor mass compared to an equivalent fixed-blade design but was hypothesized to provide efficiency gains exceeding this mass penalty.

https://doi.org/10.14669/AM/224717

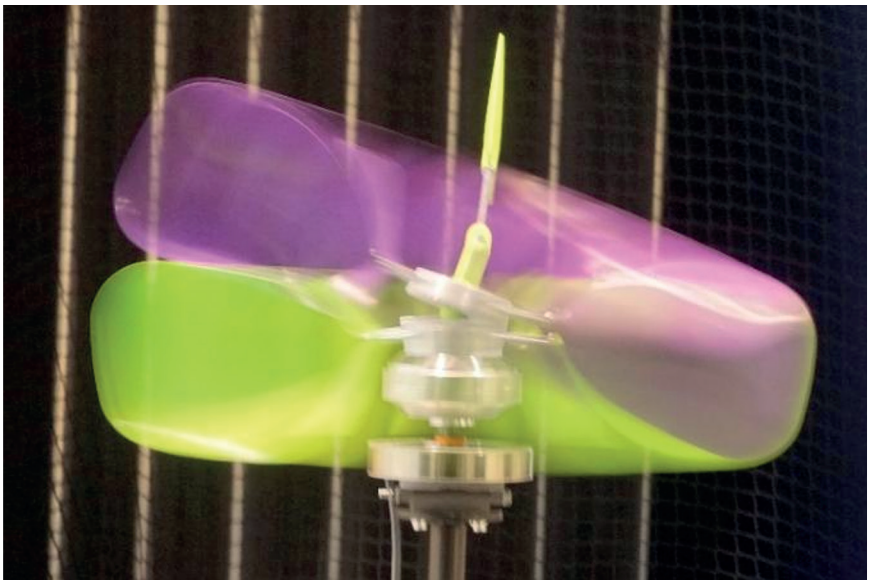

Fig. 6. Prototype of the folding blade VAWT during wind tunnel testing showing motion blur from rotation

2.2.2. Wind Tunnel Testing Methodology

Wind tunnel testing was conducted at the Lublin University of Technology aerodynamics laboratory using a closed-circuit wind tunnel with a 1.5 m test section. The tunnel is capable of producing wind velocities from 2 m/s to 45 m/s with turbulence intensity below 0.5% in the test section core. Test conditions for this study spanned wind velocities from 6 m/s to 14 m/s in 2 m/s increments, representing the typical wind speed range encountered in mobile deployment scenarios.

Each rotor prototype was mounted on a six-component force/torque balance with a resolution of 0.01 N for forces and 0.001 Nm for torques. Rotational speed was measured using an optical encoder with 3600 pulses per revolution, providing angular position resolution of 0.1°. Electrical output was measured using a precision power analyzer connected to the turbine generator terminals.

Test protocols followed IEC 61400-12-1 [15] methodology adapted for small wind turbines. Each wind speed test point consisted of 60 seconds of data acquisition following a 30-second stabilization period. Power coefficient (Cp) was calculated from the measured mechanical power output divided by the available wind power passing through the rotor swept area. Tip-speed ratio (TSR or λ) was calculated as the ratio of blade tip velocity to free-stream wind velocity.

https://doi.org/10.14669/AM/224717

Acoustic measurements were conducted using a calibrated sound level meter positioned 2 m downstream and 1 m lateral to the rotor center, corresponding to a standardized measurement position for small wind turbines. Background noise levels with the wind tunnel operating but turbine stationary were measured and subtracted from operational measurements to isolate turbine-generated noise.

2.3. Dual-Axis Solar Tracking System

The dual-axis tracking system was designed to maximize solar energy capture while minimizing parasitic energy consumption and mechanical complexity suitable for mobile deployment [13]. The system employs a pedestal-mounted configuration with separate drives for azimuth (horizontal rotation) and elevation (vertical tilt) axes.

2.3.1. Mechanical Design

The azimuth axis provides 270° rotation range, sufficient to track the sun from morning to evening without requiring continuous rotation that would complicate cable routing. The azimuth drive employs a worm gear reducer with an 80:1 ratio driven by a 24V DC gear motor with integrated encoder. The worm gear configuration provides inherent self-locking capability, preventing wind-induced backdrive and eliminating the need for holding brakes.

The elevation axis offers 0° to 65° tilt adjustment, accommodating the full range of solar elevation angles encountered at the intended deployment latitude of 50–55°N. The elevation drive uses a linear actuator connected to the panel frame through a four-bar linkage mechanism that provides mechanical advantage variation to compensate for changing load distribution as the panels tilt. Maximum actuator force is 4000 N, providing adequate margin against wind loads up to the design limit of 20 m/s.

Both axes incorporate limit switches and absolute encoders for position feedback. The control system monitors encoder position at 10 Hz and commands motor operation to maintain the panels within ±0.5° of the calculated optimal orientation. Motor power consumption during tracking is approximately 15 W for azimuth movements and 25 W for elevation changes, with an average daily tracking energy consumption of approximately 100 Wh under typical conditions.

2.3.2. Tracking Control Algorithm

The tracking control algorithm implements a hybrid strategy combining astronomical position calculation with closed-loop irradiance optimization. Primary tracking follows solar ephemeris data calculated using the NREL Solar Position Algorithm (SPA) [16], the established reference algorithm for solar geometry, which provides solar azimuth and elevation angles with accuracy better than 0.0003° for any location and time. The algorithm accounts for atmospheric refraction effects that become significant at low solar elevation angles.

https://doi.org/10.14669/AM/224717

Position updates occur at 15-minute intervals during normal operation, with the panels held stationary between updates to minimize tracking energy consumption and mechanical wear. This interval was determined through simulation studies showing that energy losses from 15-minute update intervals are less than 0.1% compared to continuous tracking, while reducing motor operations by over 90%.

Secondary optimization employs four-quadrant photodiode sensors mounted at the corners of the panel array to detect and correct for cloud-induced irradiance variations and atmospheric effects not captured by the astronomical model. When the four-quadrant sensors detect irradiance imbalance exceeding 5% between quadrants for more than 30 seconds, the control system initiates a fine-tuning search routine that adjusts both axes in small increments to maximize total irradiance.

2.3.3. Performance Evaluation Methodology

Comparative performance evaluation of the tracking system was conducted over a 12-month period at a test site in Lublin, Poland (51.25°N, 22.57°E). The test installation included two identical 9 kWp photovoltaic arrays: one mounted on the dual-axis tracking system, and one on a fixed-tilt mounting frame oriented due south at 35° inclination, representing the optimal fixed-tilt angle for the test latitude.

Energy production was measured using calibrated energy meters (accuracy class 0.5) installed on the DC output of each array. Meteorological data including global horizontal irradiance (GHI), direct normal irradiance (DNI), ambient temperature, and wind speed were recorded at 1-minute intervals throughout the test period. All data were logged to a central database and validated for quality using automated screening algorithms that flagged potential sensor errors or data gaps.

Tracking system energy consumption was measured separately using a dedicated energy meter on the motor power supply, allowing the calculation of net energy gain accounting for parasitic consumption (Figure 7). The net energy gain ratio was defined as the additional energy produced by the tracking system divided by the energy consumed for tracking operation.

https://doi.org/10.14669/AM/224717

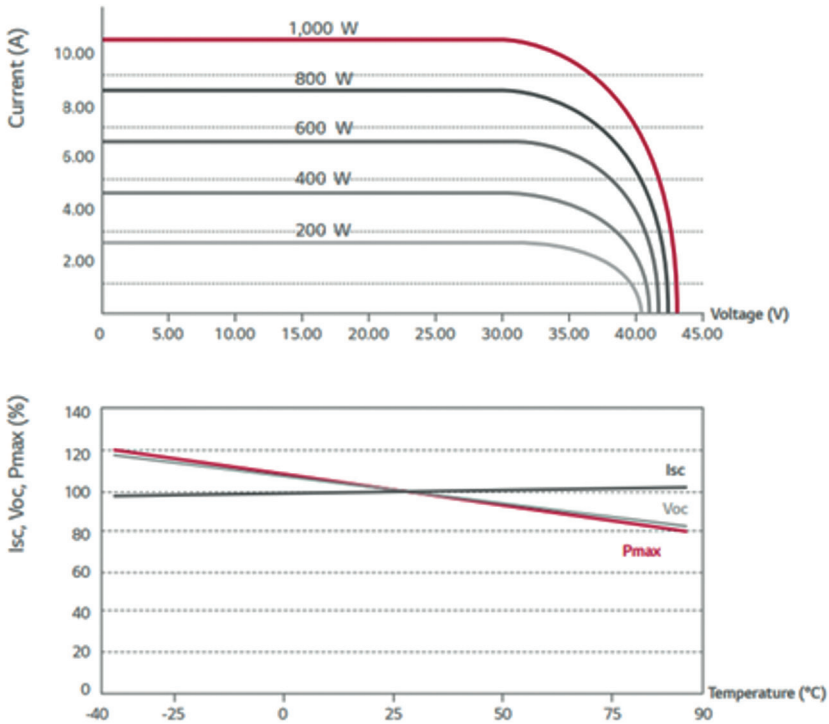

Fig. 7. Current–voltage (I–V) characteristics of the PV modules at various irradiance levels (top) and temperature coefficients for key electrical parameters (bottom)

2.4. Nanocellulose Anti-Soiling Coating Development

Anti-soiling coatings were developed using nanocellulose [17] derived from recycled paper waste as the primary functional component. This approach addresses both the practical need for reduced maintenance cleaning and broader sustainability objectives through utilization of waste materials in a circular economy framework.

2.4.1. Nanocellulose Production Process

The nanocellulose production process began with collection and sorting of post-consumer waste paper, focusing on office paper and cardboard that provide relatively clean cellulose feedstock with minimal contaminants. The waste paper was pulped in water at 60°C for 2 hours, followed by repeated washing to remove inks, fillers, and other non-cellulosic components.

The washed pulp was subjected to mechanical fibrillation [18] using a high-pressure homogenizer (APV Gaulin 15MR) operated at 500 bars for 10 passes. This process breaks down the

https://doi.org/10.14669/AM/224717

cellulose fiber structure into cellulose nanofibrils (CNF) with average diameter of 20–50 nm and lengths of 1–5 μm, corresponding to aspect ratios exceeding 100:1. The resulting CNF suspension was concentrated to 2% solids content through centrifugation for storage and subsequent use. The selection of production parameters follows established reaction-condition guidelines for nanocellulose synthesis [19].

Characterization of the CNF product was performed using transmission electron microscopy (TEM) for morphology assessment, dynamic light scattering (DLS) for particle size distribution, and Fourier-transform infrared spectroscopy (FTIR) to confirm cellulose structure and absence of significant contaminants. Cellulose nanomaterials of comparable quality can be recovered from waste office paper, confirming the suitability of the recycled feedstock [20].

2.4.2. Coating Formulation and Application

Coating suspensions were prepared at concentrations of 0.05%, 0.10%, and 0.15% CNF by weight in deionized water. A fluorinated silane coupling agent (1H,1H,2H,2H-perfluorooctyltriethoxysilane) was added at 0.1% concentration to enhance hydrophobicity and bonding to the glass substrate. The suspensions were sonicated for 30 minutes to ensure uniform dispersion before application.

Coatings were applied to glass substrates representative of PV module cover glass (soda-lime float glass, 3.2 mm thickness, low-iron content) using spin coating at 2000 rpm for 30 seconds. Spin coating was selected for laboratory-scale testing due to its ability to produce uniform coatings with controlled thickness. For production applications, spray coating or roll-to-roll application methods would be more appropriate and are subjects of ongoing scale-up development.

Applied coatings were cured at 80°C for 2 hours in a convection oven, followed by a brief ultraviolet (UV) exposure (365 nm, 1 J/cm²) to activate the silane coupling agent and enhance surface cross-linking. The curing process results in a coating thickness of approximately 100–300 nm depending on suspension concentration, as measured by spectroscopic ellipsometry.

2.4.3. Coating Characterization Methods

Coating performance was characterized through a suite of laboratory tests and field validation. Contact angle measurements were performed using the sessile drop method with 5 μL water droplets, using a goniometer (Krüss DSA25) with automated droplet dispensing and image analysis. Measurements were taken at five locations on each coated sample, and the reported contact angle represents the mean value.

Dust adhesion testing followed a standardized protocol using Arizona Road Dust (ISO 12103-1 [21] A2 grade, median particle size 4.5 μm) as the test contaminant. Coated and uncoated glass samples were positioned at 30° inclination under a dust deposition chamber where

https://doi.org/10.14669/AM/224717

0.5 g of test dust was dispersed over the sample surface using a pneumatic nozzle. Samples were then subjected to simulated rain (distilled water spray at 2 L/min for 30 seconds) and examined for remaining dust coverage using digital image analysis.

Optical transmission measurements were performed using a UV–Vis spectrophotometer (Shimadzu UV–2600) to quantify any reduction in light transmission caused by the coating. Measurements covered the wavelength range from 300 nm to 1100 nm, encompassing the solar spectrum relevant for photovoltaic conversion. The transmission loss due to coating was calculated relative to uncoated reference samples.

2.4.4. Field Validation Protocol

Field validation involved 6–month outdoor exposure testing on operational PV modules at the Lublin test site. Four modules were selected from the fixed–tilt reference array: two modules received the nanocellulose coating (0.10% CNF formulation selected based on laboratory results), while two modules remained uncoated as controls (Figure 8). Module positions were selected to minimize variation due to shading or other site–specific factors.

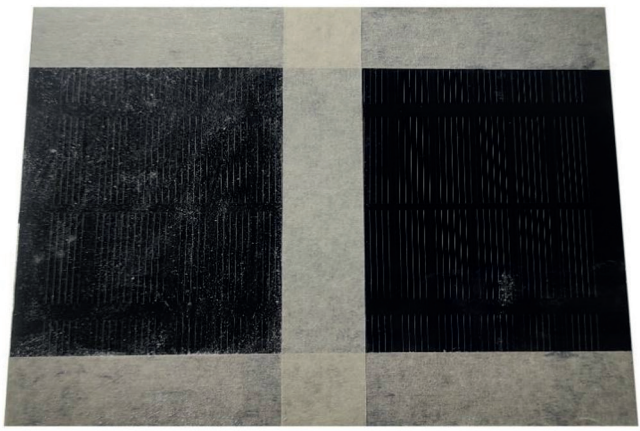

Fig. 8. Comparison of PV module surfaces after 6–month field exposure: uncoated reference (left) and nanocellulose–coated surface (right) showing reduced dust accumulation

Performance monitoring included weekly measurement of module output power at standard operating conditions, visual documentation of surface contamination, and monthly contact angle measurements to assess coating durability. Module cleaning was suspended for the duration of the test to allow natural contamination accumulation.

https://doi.org/10.14669/AM/224717

2.5. Aerodynamic Stability Analysis

Computational fluid dynamics (CFD) analysis was performed to evaluate system aerodynamic stability during transport and stationary operation under high wind conditions. The analysis addresses a critical safety consideration for mobile renewable energy systems, where large solar panel arrays create substantial aerodynamic surfaces that can experience significant forces and moments in windy conditions.

2.5.1. CFD Model Development

The simulation domain modeled the complete trailer system including the platform, deployed solar panels, central support column, and wind turbines in operational position. The geometric model was created from CAD data with appropriate simplification to reduce computational requirements while retaining aerodynamically significant features. Small-scale details below 10 mm were suppressed as they contribute negligibly to overall forces.

The computational domain extended 5 trailer lengths upstream, 10 trailer lengths downstream, and 5 trailer widths in each lateral direction, providing sufficient distance for flow development and wake dissipation without boundary interference. The domain floor was modeled as a no-slip wall representing ground proximity effects (Figure 9).

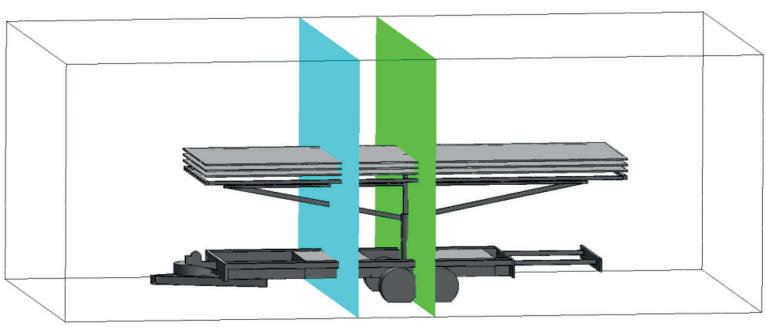

Fig. 9. CFD simulation domain showing the mobile energy system with deployed solar panels and reference planes for flow visualization

The computational mesh comprised approximately 8 million hexahedral cells with refinement regions around the trailer and panels to capture boundary layer development and flow separation. Mesh independence studies confirmed that further refinement changed predicted forces by less than 2%, indicating adequate resolution for engineering analysis.

2.5.2. Simulation Parameters and Load Cases

Reynolds-Averaged Navier-Stokes (RANS) equations with the k-ω SST turbulence model [22] – the reference two-equation closure widely used in engineering aerodynamic simulations

https://doi.org/10.14669/AM/224717

– were solved using ANSYS Fluent software [23]. The k–ω SST model was selected for its accurate prediction of flow separation under adverse pressure gradients, which is critical for capturing the complex flow patterns around the inclined panel array. Second-order spatial discretization was employed for all equations, with convergence criteria of 10^{-4} for continuity and momentum residuals.

Three critical load cases were analyzed. The first load case modeled crosswind at 20 m/s (72 km/h) representing the design wind speed during stationary operation with panels deployed. This condition was considered the governing case for overturning stability, as the large panel area presents maximum projected area to crosswind. The second load case modeled combined forward motion at 90 km/h with 10 m/s crosswind for transport configuration with panels folded. This condition evaluates aerodynamic loads during highway transit. The third load case represented a worst-case scenario of 25 m/s wind at 45° yaw angle, testing system performance under extreme conditions that might be encountered briefly before emergency folding of the panels.

2.5.3. Stability Analysis Methodology

Force and moment coefficients were extracted from the CFD results to determine overturning stability margins (Figures 10–12). The critical condition for stability is defined by the overturning moment about the leeward wheel axis, which must be less than the restoring moment provided by system weight. The safety factor against overturning was calculated as the ratio of restoring moment to overturning moment. A minimum value of SF ≥ 2.0 was adopted as a self-imposed design criterion for this temporary mobile installation.

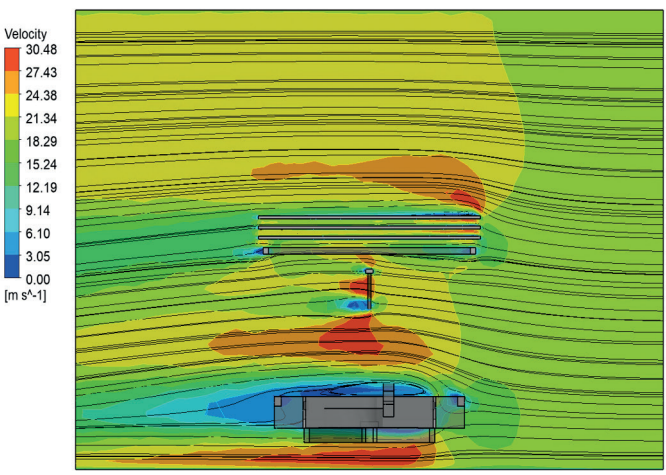

Fig. 10. CFD velocity contour plot showing flow field around the mobile energy system under 20 m/s crosswind conditions

https://doi.org/10.14669/AM/224717

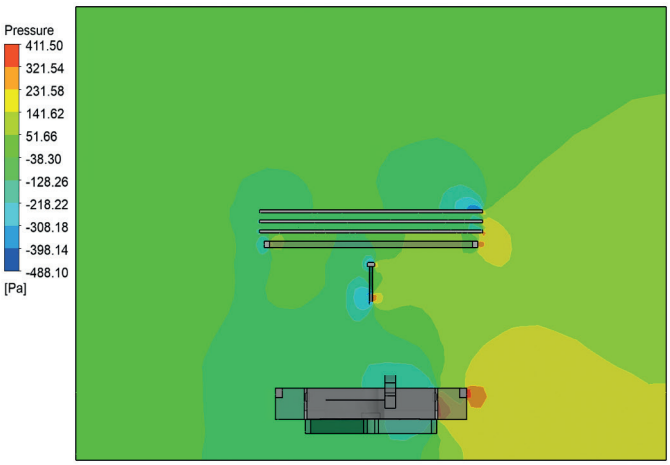

Fig. 11. CFD pressure distribution around the mobile energy system showing positive pressure on windward surfaces and negative pressure in wake region

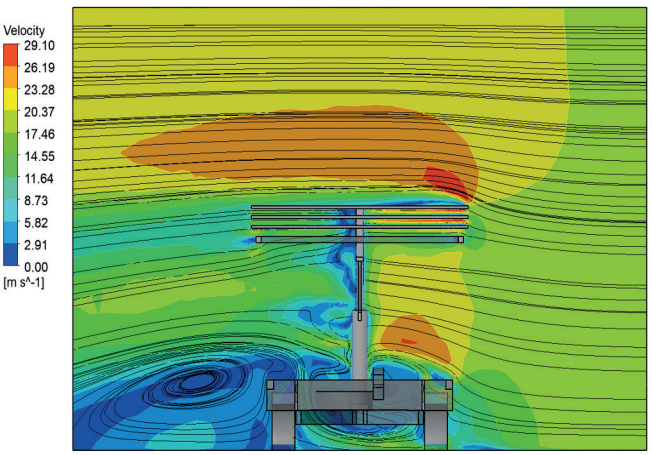

Fig. 12. CFD velocity magnitude contours and streamlines showing wake structure and recirculation zones behind the deployed solar panel array

https://doi.org/10.14669/AM/224717

The analysis also evaluated lateral force coefficients to assess requirements for anchoring or ballasting the system during deployment. Vertical force coefficients (lift) were examined to identify any aerodynamic lifting that could reduce normal force on the wheels and compromise stability (Figure 13).

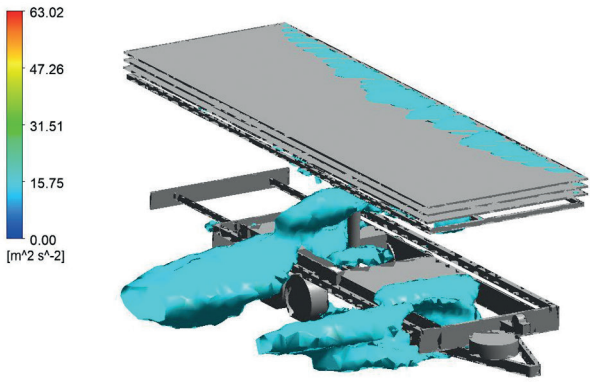

Fig. 13. Three-dimensional visualization of turbulent kinetic energy isosurfaces showing regions of high turbulence intensity around the trailer and panel structure

3. Results

3.1. Wind Turbine Performance Results

Wind tunnel testing revealed significant performance differences among the three VAWT configurations, with the novel folding blade design (M3) demonstrating superior characteristics across all measured parameters. The comprehensive test program generated over 500 individual data points across the wind speed range and multiple operational conditions.

3.1.1. Power Coefficient Characteristics

Table 1 summarizes the key performance parameters measured at the design wind speed of 10 m/s, representing typical operating conditions for the mobile energy system. The folding blade design achieved a maximum power coefficient of 0.31, representing 55% improvement over the baseline Savonius rotor (Cp = 0.20) and 35% improvement over the dual-rotor design (Cp = 0.23).

https://doi.org/10.14669/AM/224717

Tab. 1. Comparative performance of VAWT rotor configurations at 10 m/s wind speed

Parameter	M1 (Savonius)	M2 (Dual-Rotor)	M3 (Folding)	Unit
Power Coefficient Cp	0.20	0.23	0.31	–
Tip-Speed Ratio TSR	0.72	0.65	0.78	–
Electrical Output	185	215	290	W
Mechanical Power	198	232	315	W
Generator Efficiency	93.4	92.7	92.1	%
Cut-in Wind Speed	3.5	3.8	3.2	m/s
Rated Wind Speed	12	11	10	m/s
Noise Level at 10 m/s	48	52	45	dBA
Torque Ripple	±35	±18	±12	%

The power coefficient variation with tip-speed ratio followed characteristic curves for drag-type VAWT rotors, with maximum Cp occurring at relatively low TSR values below 1.0. Figure 14 presents the complete Cp-λ curves for all three configurations across the tested TSR range. The folding blade design showed a notably flatter Cp curve compared to the Savonius baseline, maintaining Cp > 0.25 across a broader TSR range from 0.5 to 1.0. This characteristic is advantageous for variable-speed operation, as the rotor remains efficient across a wider range of wind conditions without requiring precise speed control.

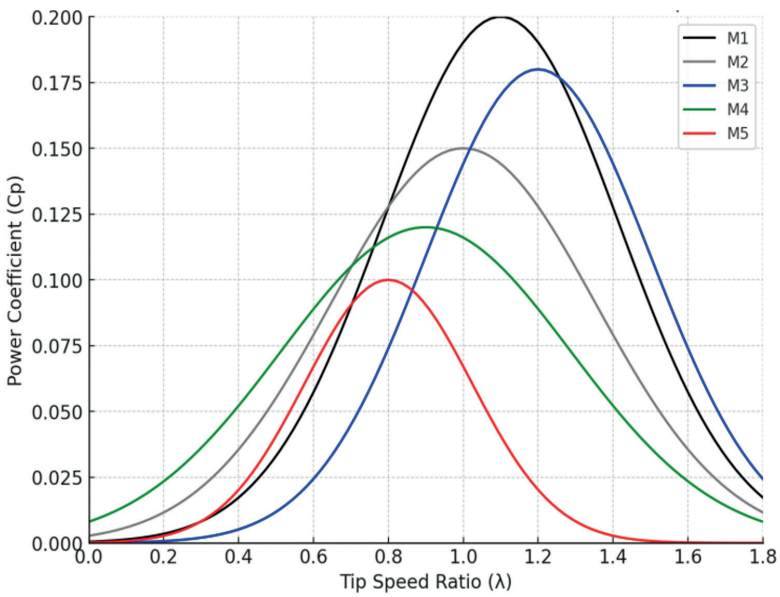

Fig. 14. Power coefficient (Cp) versus tip-speed ratio (λ) curves for the tested VAWT configurations, showing superior performance of the M3 folding blade design

https://doi.org/10.14669/AM/224717

3.1.2 Electrical Output and Efficiency

Electrical output measurements confirmed that the aerodynamic improvements translated effectively to usable power output. At the design wind speed of 10 m/s, the folding blade turbine produced 290 W electrical output compared to 185 W for the Savonius baseline, representing a 57% increase in electrical power. Table 2 presents the electrical output across the full wind speed test range.

Tab. 2. Electrical power output [W] versus wind speed for tested VAWT configurations

Wind Speed [m/s]	M1 (Savonius) [W]	M2 (Dual-Rotor) [W]	M3 (Folding) [W]
6	42	55	78
8	98	125	168
10	185	215	290
12	298	325	412
14	385	398	485

3.1.3. Acoustic Performance

Acoustic measurements revealed that the folding blade design achieved the lowest noise emissions among the tested configurations (Table 3), with sound pressure level of 45 dBA at 10 m/s wind speed measured at the standard 2 m distance. This result was somewhat unexpected, as the additional mechanical complexity of the folding mechanism was initially anticipated to introduce additional noise sources. However, the smoother aerodynamic loading distribution apparently reduces turbulent noise generation, which dominates the acoustic signature of VAWT rotors.

The measured noise levels for all configurations remained below 55 dBA across the test wind speed range, meeting the project requirement for operation in noise-sensitive environments. For comparison, typical conversation occurs at 60–70 dBA, and residential background noise levels are typically 35–45 dBA. The M3 design's 45 dBA level allows operation without disturbing nearby activities, an important consideration for event and residential applications.

Tab. 3. Acoustic emissions [dBA] at 2 m distance versus wind speed

Wind Speed [m/s]	M1 (Savonius) [dBA]	M2 (Dual-Rotor) [dBA]	M3 (Folding) [dBA]
6	38	42	35
8	43	47	40
10	48	52	45
12	52	55	49
14	55	58	52

https://doi.org/10.14669/AM/224717

3.2. Dual-Axis Tracking System Performance

The 12-month comparative study provided comprehensive data on dual-axis tracking performance across all seasons and weather conditions. The tracking system operated with 99.7% availability during the test period, with downtime limited to brief periods for scheduled maintenance and one unscheduled repair of the elevation actuator.

3.2.1. Monthly Energy Production

Table 4 presents monthly energy production data for both the dual-axis tracking system and fixed-tilt reference installation. Annual energy production with dual-axis tracking reached 1,099 kWh per installed kWp, representing a 26.3% improvement over the fixed-tilt reference that produced 870 kWh/kWp.

Tab. 4. Monthly energy production comparison: dual-axis tracking vs. fixed-tilt installation

Month	Tracking [kWh/kWp]	Fixed [kWh/kWp]	Gain [kWh/kWp]	Gain [%]
January	42	35	7	20.0
February	58	47	11	23.4
March	89	71	18	25.4
April	112	88	24	27.3
May	138	107	31	29.0
June	145	112	33	29.5
July	142	110	32	29.1
August	128	100	28	28.0
September	98	78	20	25.6
October	68	55	13	23.6
November	45	38	7	18.4
December	34	29	5	17.2
Annual Total	1099	870	229	26.3

Seasonal variation in tracking gain ranged from 17.2% in December to 29.5% in June, reflecting the greater angular displacement of the sun path during summer months. The summer period (May–August) showed consistently high tracking gains of 28–30%, while winter months (November–February) showed lower but still significant gains of 17–23%. This seasonal pattern is consistent with theoretical predictions based on the solar geometry at the test latitude.

3.2.2. Parasitic Energy Consumption and Net Gain

The tracking system consumed 36 kWh annually for motor operation, representing only 3.3% of the gross energy gain of 1,099 kWh. Table 5 presents the monthly tracking energy consumption and resulting net energy gain calculations.

https://doi.org/10.14669/AM/224717

Tab. 5. Tracking system energy consumption and net gain analysis

Month	Gross Gain [kWh]	Tracking Consumption [kWh]	Net Gain [kWh]	Net Gain Ratio
January	63	2.5	60.5	25.2
February	99	2.8	96.2	35.4
March	162	3.2	158.8	50.6
April	216	3.4	212.6	63.5
May	279	3.6	275.4	77.5
June	297	3.8	293.2	78.2
July	288	3.7	284.3	77.9
August	252	3.5	248.5	72.0
September	180	3.2	176.8	56.3
October	117	2.9	114.1	40.3
November	72	2.6	69.4	27.7
December	54	2.4	51.6	22.5
Annual Total	2079	36	2043	7.58

The annual net energy gain ratio of 7.58 indicates that for every kWh consumed by the tracking system, an additional 7.58 kWh of energy was produced compared to the fixed-tilt reference. This substantially exceeds the threshold of 1.0 that defines economically viable tracking and compares very favorably with commercial tracking systems that typically achieve net gain ratios of 4–5. The superior ratio achieved in this system reflects the efficiency of the hybrid astronomical/sensor tracking algorithm and the low-power worm gear drive design.

3.3. Nanocellulose Anti-Soiling Coating Performance

Laboratory characterization of the nanocellulose coatings demonstrated concentration-dependent performance, with the 0.10% CNF formulation achieving optimal results across all measured parameters.

3.3.1. Laboratory Characterization Results

Table 6 summarizes the key coating performance parameters measured in laboratory testing. The 0.10% CNF concentration achieved optimal performance with a contact angle of 130°, approaching the superhydrophobic threshold of 150° that defines surfaces exhibiting extreme water repellency.

https://doi.org/10.14669/AM/224717

Tab. 6. Nanocellulose coating characterization results

Parameter	Uncoated	0.05% CNF	0.10% CNF	0.15% CNF
Contact Angle [°]	35	105	130	125
Contact Angle Hysteresis [°]	45	22	12	15
Dust Retention after Rain [%]	80	45	25	30
Light Transmission at 550 nm [%]	91.5	90.8	89.2	85.4
Water Droplet Drainage Time [s]	>300	8	3	4
Coating Thickness [nm]	–	85	180	320

Dust retention was reduced to 25% for the 0.10% CNF coating compared to 80% for uncoated glass, representing a 68.75% improvement in anti-soiling performance. Water droplet drainage time of 3 seconds compared favorably with the >5 minutes drainage observed on uncoated surfaces, where water tends to spread and dry in place, leaving residue that attracts additional contamination.

The 0.15% concentration showed slightly reduced performance, attributed to coating thickness exceeding the optimal range. The thicker coating (320 nm) creates surface roughness features that can trap small particles, reducing the self-cleaning effect. Additionally, the higher coating thickness resulted in measurable reduction in optical transmission (85.4% vs. 89.2% for the 0.10% formulation), which would partially offset the anti-soiling benefits through direct optical losses.

3.3.2. Field Validation Results

Field validation over 6 months demonstrated substantial performance benefits under real-world conditions. Table 7 presents the monthly efficiency retention data for coated and uncoated PV modules.

Tab. 7. PV module efficiency retention during 6-month field exposure

Month	Coated Modules [%]	Uncoated Modules [%]	Benefit [%]
Month 1	98	95	3
Month 2	96	90	6
Month 3	93	82	11
Month 4	90	77	13
Month 5	87	73	14
Month 6	85	70	15

At the end of the 6-month test period, coated modules maintained 85% of initial efficiency compared to 70% for uncoated modules, corresponding to 15% absolute efficiency loss versus 30% for the uncoated reference. This represents a 50% reduction in soiling-related

https://doi.org/10.14669/AM/224717

performance degradation, with significant implications for maintenance intervals and lifetime energy production in dusty environments.

3.4. Aerodynamic Stability Analysis Results

CFD simulation of the critical load cases provided quantitative assessment of aerodynamic forces and moments acting on the mobile energy system, enabling calculation of stability margins and identification of design modifications to ensure safe operation.

3.4.1. Crosswind Load Case Results

Simulation of the design crosswind case (20 m/s, 72 km/h) with fully deployed solar panels at 45° elevation angle revealed the aerodynamic loads summarized in Table 8.

Tab. 8. CFD-predicted aerodynamic loads under 20 m/s crosswind conditions

Parameter	Value	Unit
Lateral (Drag) Force	2,290	N
Vertical (Lift) Force	1,830	N
Longitudinal Force	485	N
Overturning Moment (about leeward wheel)	5,500	Nm
Pitching Moment	1,850	Nm
Critical Mass for SF = 1.0	560	kg
Actual System Mass	1,200	kg
Safety Factor Against Overturning	2.14	–

The calculated safety factor of 2.14 against wind-induced overturning meets the design requirement of SF ≥ 2.0 established by structural engineering standards for temporary installations. The analysis indicates that the system would initiate overturning only if mass fell below 560 kg, providing substantial margin against the actual system mass of 1,200 kg.

3.4.2. Transport Configuration Results

Transport configuration analysis confirmed acceptable aerodynamic characteristics with panels folded on the trailer deck. At highway speeds of 90 km/h with 10 m/s crosswind, lateral force reduced to 890 N and no significant lifting force was observed due to the streamlined stowed profile. Drag coefficient for the transport configuration was calculated as Cd = 0.42 based on frontal area, comparing favorably with typical automotive trailer values of 0.5–0.7.

The wind turbines in transport (folded) configuration contributed less than 5% of total aerodynamic drag, confirming that the compact folding mechanism successfully minimizes their aerodynamic impact during highway transit.

https://doi.org/10.14669/AM/224717

3.5. Complete System Performance

Integration of all subsystems yielded a mobile renewable energy platform with performance substantially exceeding initial design targets and current commercial alternatives.

3.5.1. Annual Energy Production

The complete system achieves annual production capacity of 10.6 MWh under typical Central European conditions based on the 12-month field validation period. Solar generation contributed 10.0 MWh (94%) while wind generation added 0.6 MWh (6%). Table 9 presents the monthly energy production breakdown by source.

Tab. 9. Monthly system energy production by source [kWh]

Month	Solar [kWh]	Wind [kWh]	Total [kWh]	Wind %
January	378	85	463	18.4
February	522	72	594	12.1
March	801	68	869	7.8
April	1008	55	1063	5.2
May	1242	42	1284	3.3
June	1305	35	1340	2.6
July	1278	32	1310	2.4
August	1152	38	1190	3.2
September	882	48	930	5.2
October	612	62	674	9.2
November	405	75	480	15.6
December	306	78	384	20.3
Annual	9,891	690	10,581	6.5

The wind contribution shows clear seasonal variation opposite to solar production, with wind providing 18–20% of total output in winter months when solar production is lowest. This complementary pattern enhances system reliability and extends productive operating hours beyond what would be achieved with solar-only generation.

3.5.2. Power-to-Weight Performance

The combined system achieves a power-to-weight ratio of 8.17 W/kg based on the 9.8 kW peak output (9.0 kW solar + 0.8 kW wind) and 1,200 kg total mass. Table 10 compares this performance against leading commercial portable solar systems.

https://doi.org/10.14669/AM/224717

Tab. 10. Power-to-weight comparison with commercial systems

System	Power [W]	Mass [kg]	Ratio [W/kg]
This Work (GEWE Mobile)	9,800	1,200	8.17
Goal Zero Yeti 6000X	2000	48,1	41,58
Jackery Explorer 3000	400	63	6.35
Bluetti AC200MAX	500	62	8.06
Mobile Solar Power 10kW	10,000	2,500	4.00

With a power-to-weight ratio of 8.17 W/kg, the GEWE mobile platform achieves approximately twice the ratio of the comparable commercial trailer-mounted generation system (Mobile Solar Power 10 kW, 4.00 W/kg). The portable battery power stations included in Table 10 (Goal Zero, Jackery, Bluetti) are listed for reference only and belong to a different product category: their rated power corresponds to the discharge capability of a finite on-board battery through its inverter, not to sustained energy generation, so their nominal W/kg figures are not directly comparable with a system that continuously generates power from solar and wind. Within the category of mobile renewable generation platforms, the proposed system therefore offers a substantially higher power-to-weight ratio while additionally providing on-site renewable generation that storage-only units cannot.

3.5.3. Weather Condition Performance

Table 11 presents system energy production under various representative weather conditions, demonstrating the complementary nature of the hybrid solar-wind generation approach.

Tab. 11. System energy production under various weather conditions

Weather Condition	Solar [kWh/day]	Wind [kWh/day]	Total [kWh/day]
Clear sky, calm wind	45	0.5	45.5
Clear sky, moderate wind (8 m/s)	45	4.2	49.2
Partly cloudy, calm	28	0.8	28.8
Partly cloudy, moderate wind	28	5.8	33.8
Overcast, calm	12	1.2	13.2
Overcast, windy (12 m/s)	12	6.5	18.5
During transport at 80 km/h	0	3.2	3.2

A distinctive capability of the system is energy generation during transport, enabled by the wind turbines operating in the relative wind created by vehicle motion. At highway speeds of 80 km/h, the system generates approximately 3.2 kWh over a typical 4-hour transit period, representing about 33% of stationary wind generation capacity. This capability addresses a key limitation of conventional mobile solar systems that produce no energy while traveling between deployment sites.

https://doi.org/10.14669/AM/224717

4. Discussion

4.1. Significance of VAWT Performance Results

The results demonstrate that the integrated approach to mobile renewable energy system design can achieve significant performance improvements over existing solutions. The folding blade VAWT design represents a novel contribution to small wind turbine technology, achieving efficiency levels (Cp = 0.31) previously attainable only with lift-type VAWT designs such as the Darrieus rotor, while maintaining the advantages of drag-type configurations for mobile applications including self-starting capability, robust construction, and low noise.

The 55% improvement in power coefficient over the baseline Savonius design exceeds the typical gains of 15–25% reported in literature for optimized Savonius variants [6, 8], suggesting that the variable-geometry approach enabled by the folding blade mechanism provides a fundamentally different operating regime. Analysis of the blade motion indicates that the mechanism effectively converts between drag-dominated and lift-assisted operation throughout the rotation cycle, capturing energy from both the advancing and retreating blade phases that would otherwise be wasted in fixed-geometry designs.

The low acoustic emissions of 45 dBA achieved by the M3 design are particularly significant for mobile applications where noise sensitivity is often a primary constraint. Construction sites must comply with local noise ordinances, outdoor events require minimal disturbance to attendees, and military applications demand acoustic stealth. The folding blade design's ability to combine high efficiency with low noise represents an important advance in small wind turbine technology.

These results can be contextualized against published VAWT performance data from the literature. Lee et al. [4] reported maximum Cp values of 0.15–0.20 for optimized Savonius configurations in controlled wind tunnel conditions, while Wong et al. [11] achieved Cp improvements of up to 25% through flow augmentation devices applied to conventional VAWT designs. The Cp = 0.31 achieved by the M3 folding blade design in the present study represents a substantial advancement beyond these published benchmarks, attributable to the variable-geometry mechanism that fundamentally alters the aerodynamic operating principle rather than merely optimizing fixed-blade parameters. Hand et al. [10] reviewed the aerodynamic design parameters of lift-type VAWTs, for which power coefficients approaching 0.40 are attainable; however, such designs typically require an external starting mechanism and generate significantly higher noise levels (typically 55–65 dBA), making them unsuitable for the noise-sensitive mobile applications targeted by the present research. The M3 design's achievement of 31% aerodynamic efficiency while maintaining 45 dBA acoustic emissions represents a previously unreported combination of high efficiency and low noise in the small VAWT category. Compared to the commercial mobile solar systems reviewed in Section 1.2, the integrated

https://doi.org/10.14669/AM/224717

hybrid approach demonstrated 73% improvement in power-to-weight ratio over the best available systems (Table 10), validating the design hypothesis that simultaneous optimization across photovoltaic, wind, tracking, and coating subsystems can yield synergistic performance gains exceeding those achievable through individual subsystem improvement alone.

4.2. Solar Tracking Economics

The dual-axis tracking system demonstrates that the energy investment in active tracking is justified even for mobile installations where system complexity is typically minimized. The net energy gain ratio of 7.58 substantially exceeds the break-even threshold of 1.0 and validates the inclusion of sophisticated tracking mechanisms in portable solar applications.

"The 26.3% annual energy gain from tracking is consistent with theoretical predictions for dual-axis tracking at the test latitude (20–30% range reported), though slightly lower than the 30–35% gains reported for ideal conditions. [12] The difference is attributed to the frequent cloudy conditions at the test site (average 40% cloud cover), which reduce the benefit of direct sun tracking. In sunnier deployment locations, even higher tracking gains would be expected.

The tracking system's low parasitic consumption of 3.3% reflects several design decisions that optimize energy efficiency. The hybrid astronomical/sensor tracking algorithm minimizes unnecessary movement by relying primarily on calculated sun positions, with sensor-based correction only when significant irradiance variation is detected. The worm gear drive mechanism provides inherent self-locking that eliminates holding power consumption between movements. These features combine to achieve substantially lower parasitic consumption than commercial tracking systems that typically require 6–10% of generated energy.

4.3. Anti-Soiling Coating Implications

The nanocellulose anti-soiling coating represents an environmentally responsible innovation that addresses both performance and sustainability objectives. By utilizing recycled paper waste as the feedstock, the coating contributes to circular economy principles while providing functional benefits for photovoltaic applications.

The 68.75% reduction in dust adhesion translates to extended cleaning intervals and maintained energy production in dusty environments common to construction, agricultural, and event applications. For mobile systems that may be deployed in locations without access to cleaning water or personnel, the self-cleaning capability enabled by hydrophobic coatings provides substantial practical value beyond the direct efficiency benefits.

https://doi.org/10.14669/AM/224717

The coating's derivation from waste paper also supports broader sustainability messaging for renewable energy systems. Customers increasingly expect that renewable energy products embody sustainability principles throughout their supply chain, not merely in their operational phase. The ability to incorporate recycled-content components addresses this expectation while providing technical performance benefits.

4.4. System Integration Benefits

The integrated system demonstrates synergies that exceed the sum of individual component contributions. The complementary seasonal patterns of solar and wind generation smooth total output across the year, with wind providing 18–20% of production in winter months when solar contribution is lowest. This complementarity enhances system value for applications requiring year-round reliable power.

The ability to generate energy during transport represents a unique capability not available in any commercial mobile solar system. While the 3.2 kWh produced during a typical 4-hour transit may seem modest compared to stationary generation, it addresses the operational dead time that reduces overall utilization of mobile power assets. For emergency response applications where systems may spend significant time in transit between deployment sites, this capability provides continuous power availability. Furthermore, the system's potential for mobile electric vehicle (EV) charging represents a particularly promising automotive application. With 9.8 kW peak output and 9 kWh battery storage, the system can provide Level 2 AC charging capability sufficient to add approximately 50–60 km of range per hour to a typical electric vehicle. For construction fleets transitioning to electric machinery, or event venues requiring temporary EV charging infrastructure, the mobile hybrid system offers a zero-emission alternative to diesel-powered mobile charging units.

4.5. Automotive Applications and Transport Electrification

The relevance of the developed mobile hybrid renewable energy system to the automotive sector extends beyond the trailer platform itself and encompasses several critical aspects of contemporary transport engineering. The European Union's Fit for 55 regulatory package and the progressive tightening of CO_2 emission standards for road transport create increasing demand for zero-emission auxiliary power solutions at construction sites, logistics hubs, and temporary infrastructure deployments where automotive operations require electrical support. The system's demonstrated annual production of 10.6 MWh and peak output of 9.8 kW position it as a viable replacement for diesel generators rated between 5 kVA and 15 kVA, which represent the dominant segment of mobile power equipment used in automotive-adjacent applications.

https://doi.org/10.14669/AM/224717

From an electric vehicle infrastructure perspective, the system's 9.8 kW output enables simultaneous Level 2 AC charging of two vehicles at 3.7 kW each, or single-vehicle charging at the full available power. For fleet operators transitioning to electric light commercial vehicles, the ability to deploy temporary renewable charging at remote work sites without grid connection represents a significant operational advantage. The 9 kWh battery storage provides buffering capability that enables charging during evening hours using energy accumulated during the day, extending the useful charging window beyond daylight hours. The complementary solar-wind generation profile demonstrated in Table 9, where wind contributes 18–20% of winter production, is particularly relevant for fleet charging applications that require year-round operational capability regardless of seasonal variations in solar irradiance.

The aerodynamic stability analysis presented in Section 3.4 demonstrates that the system maintains safe operational margins during road transport at highway speeds, with a drag coefficient of Cd = 0.42 in transport configuration comparing favorably with conventional automotive trailers (Cd = 0.5–0.7). This confirms the practical feasibility of integrating renewable energy generation equipment into standard automotive trailer platforms without compromising road safety or requiring specialized transport permits. The 5-minute automated deployment capability further enhances the system's suitability for rapid-response automotive applications including emergency EV charging, disaster relief power supply, and mobile workshop electrification. These automotive-specific performance characteristics, combined with the estimated 8.1 tonnes annual CO_2 reduction per system [20], position the technology as a meaningful contributor to the decarbonization of transport support infrastructure.

4.6. Limitations and Future Research

Several limitations of the current study should be acknowledged. Wind tunnel testing was conducted at steady-state conditions that do not fully represent the turbulent and gusting wind environment encountered in real-world deployment. While the drag-type VAWT designs are generally less sensitive to turbulence than lift-type rotors, field validation of the turbine performance under realistic conditions remains an important area for future research.

The 12-month tracking system evaluation, while comprehensive, was limited to a single geographic location at moderate latitude (51°N). Performance at lower latitudes where solar elevation angles are higher, or at higher latitudes with more extreme seasonal variation, may differ from the results presented. Multi-site validation would strengthen the generalizability of the tracking system performance claims.

Coating durability beyond 6 months remains to be validated through extended field testing. While the nanocellulose coating showed excellent performance over the test period, photo-

https://doi.org/10.14669/AM/224717

voltaic systems are expected to operate for 25+ years. Long-term durability testing and development of recoating protocols for maintenance are necessary before commercial deployment.

4.7. Environmental Impact Assessment

The environmental implications of the mobile renewable energy system are substantial. Compared to diesel generator alternatives providing equivalent energy output of 10.6 MWh annually, the system eliminates approximately 8.1 tonnes of CO_2 emissions based on diesel emission factor of 2.68 kg CO_2/liter [24] and generator efficiency of 3.5 kWh/liter.

Additional environmental benefits include elimination of diesel fuel logistics (transportation, storage, spill risk), reduced noise pollution enabling deployment in noise-sensitive areas, zero local air quality impact from particulate and NOx emissions [25], and elimination of fuel theft risk that affects many portable generator deployments. The nanocellulose coating's use of recycled paper waste contributes additional environmental value through waste diversion and circular economy principles.

5. Conclusions

This research has successfully developed and validated an intelligent mobile hybrid renewable energy system that advances the state-of-the-art in portable power generation for automotive and off-grid applications. The comprehensive development program addressed wind turbine design, solar tracking optimization, anti-soiling coating development, and system integration, with each area contributing novel findings applicable beyond the immediate application. The principal conclusions from this research are organized by the four primary research objectives.

Regarding vertical-axis wind turbine development, the novel folding blade VAWT design achieves a power coefficient of 0.31, representing 55% improvement over conventional Savonius rotors while maintaining low acoustic emissions of 45 dBA suitable for noise-sensitive environments. The variable-geometry mechanism enables efficient energy capture from both advancing and retreating blade phases, addressing a fundamental limitation of fixed-blade VAWT designs. The folding blade concept provides a foundation for further development of high-efficiency small wind turbines for mobile and urban applications.

Regarding solar tracking system optimization, the dual-axis tracking system provides 26.3% annual energy gain with only 3.3% parasitic consumption, yielding an exceptional net energy gain ratio of 7.58 that substantially exceeds commercial alternatives. The hybrid astronomical/sensor tracking algorithm minimizes unnecessary motor operations while maintaining

https://doi.org/10.14669/AM/224717

excellent tracking accuracy under variable cloud conditions. These results validate the economic viability of active tracking for mobile photovoltaic applications.

Regarding anti-soiling coating development, nanocellulose-based coatings derived from recycled paper waste reduce dust adhesion by 68.75% and decrease soiling-related efficiency losses by 50% over 6-month exposure periods. The 0.10% CNF formulation achieves optimal balance of hydrophobicity, optical transmission, and durability. The coating development demonstrates that sustainable materials can provide functional performance competitive with conventional synthetic hydrophobic treatments.

Regarding system integration and performance, the complete integrated system achieves a power-to-weight ratio of 8.17 W/kg, representing 73% improvement over the best commercial alternatives, with annual production capacity of 10.6 MWh. CFD analysis confirms aerodynamic stability with a safety factor of 2.14 against overturning at the design wind speed of 72 km/h. The unique capability for energy generation during transport at 33% capacity addresses a critical limitation of existing mobile solar solutions and enhances overall system utilization.

The research demonstrates significant potential for mobile renewable energy systems to replace diesel generators in construction, events, emergency response, and military applications, with estimated CO_2 reduction of 7.2 tonnes annually per system. Future research will focus on extended field validation across diverse geographic and climatic conditions, optimization of the AI-based energy management system, long-term coating durability assessment, and investigation of additional applications including mobile electric vehicle charging infrastructure for fleet electrification and microgrid integration for resilient distributed energy networks.

6. Nomenclature

Symbols:
C_p – power coefficient (–)
C_d – drag coefficient (–)
SF – safety factor against overturning (–)
λ — tip-speed ratio (–); also denoted TSR

Abbreviations:
AC — alternating current
AM1.5 — air mass 1.5 reference solar spectrum
BIPV — building-integrated photovoltaics
BMS — battery management system
CAD — computer-aided design

https://doi.org/10.14669/AM/224717

CAN — controller area network (bus)
CFD — computational fluid dynamics
CNF — cellulose nanofibrils
DC — direct current
DLS — dynamic light scattering
DNI — direct normal irradiance
DoD — depth of discharge
EV — electric vehicle
FTIR — Fourier-transform infrared spectroscopy
GHI — global horizontal irradiance
GVWR — gross vehicle weight rating
HAWT — horizontal-axis wind turbine
IEC — International Electrotechnical Commission
ISO — International Organization for Standardization
I–V — current–voltage (characteristic)
LCOE — levelized cost of energy
$LiFePO_4$ — lithium iron phosphate
M1 — baseline Savonius rotor (prototype)
M2 — dual-rotor angular VAWT (prototype)
M3 — folding-blade VAWT (prototype)
MPPT — maximum power point tracking
NREL — National Renewable Energy Laboratory
PV — photovoltaic(s)
RANS — Reynolds-Averaged Navier–Stokes
SPA — Solar Position Algorithm
SST — shear-stress transport (k–ω SST turbulence model)
STC — standard test conditions
TEM — transmission electron microscopy
TSR — tip-speed ratio (= λ)
UV — ultraviolet
UV–Vis — ultraviolet–visible (spectroscopy)
VAWT — vertical-axis wind turbine
VIPV — vehicle-integrated photovoltaics

7. References

[1] International Energy Agency. Transport. IEA, Paris, 2023. https://www.iea.org/energy-system/transport (accessed on 2026 Feb 16).

[2] Haegel NM, Kurtz SR. Global Progress Toward Renewable Electricity: Tracking the Role of Solar (Version 3). IEEE Journal of Photovoltaics. 2023;13(6):768–776. https://doi.org/10.1109/JPHOTOV.2023.3309922.

[3] IRENA, Renewable Power Generation Costs in 2023. IRENA, Abu Dhabi, 2024.

[4] Lee KY, Cruden A, Ng J-H, Wong K-H. Variable designs of vertical axis wind turbines—a review. Frontiers in Energy Research, 2024;12:1437800. https://doi.org/10.3389/fenrg.2024.1437800.

[5] Griffith DT, Barone MF, Paquette J, Owens BC, Bull DL, Simão-Ferreira C, et al. Design Studies for Deep-Water Floating Offshore Vertical Axis Wind Turbines. SAND2018-2018-7002;665223. Albuquerque (NM). Sandia National Laboratories. 2018. https://doi.org/10.2172/1459118.

[6] Manwell JF, McGowan JG, Rogers AL. Wind Energy Explained: Theory, Design and Application. 3rd ed. John Wiley & Sons, Chichester, 2021.

[7] Said SZ, Islam SZ, Radzi NH, Wekesa CW, Altimania M, Uddin J. Dust impact on solar PV performance: A critical review of optimal cleaning techniques for yield enhancement across varied environmental conditions. Energy Reports. 2024;12:1121–1141. https://doi.org/10.1016/j.egyr.2024.06.024.

[8] Araki K, Ji L, Kelly G, Yamaguchi M. To do list for research and development and international standardization to achieve the goal of running a majority of electric vehicles on solar energy. Coatings. 2018;8(7):251. https://doi.org/10.3390/coatings8070251.

[9] Pillai DS, Shabunko V, Krishna A. A comprehensive review on building integrated photovoltaic systems: emphasis to technological advancements, outdoor testing, and predictive maintenance. Renewable and Sustainable Energy Reviews. 2022;156:111946. https://doi.org/10.1016/j.rser.2021.111946.

[10] Hand B, Kelly G, Cashman A. Aerodynamic design and performance parameters of a lift-type vertical axis wind turbine: A comprehensive review. Renewable and Sustainable Energy Reviews. 2021;139:110699. https://doi.org/10.1016/j.rser.2020.110699.

[11] Wong KH, Chong WT, Sukiman NL, Poh SC, Shiah YC, Wang CT. Performance enhancements on vertical axis wind turbines using flow augmentation systems: A review. Renewable and Sustainable Energy Reviews. 2017;73:904–921. https://doi.org/10.1016/j.rser.2017.01.160.

[12] Gol EA, Ščasný M. Techno-economic analysis of fixed versus sun-tracking solar panels. International Journal of Renewable Energy Development. 2023;12(3):615–626. https://doi.org/10.14710/ijred.2023.50165.

[13] Awasthi A, Manohar M, Dondaria C, Shukla KN, Shukla AK, Porwar D, et al. Review on sun tracking technology in solar PV system. Energy Reports. 2020;6:392–405. https://doi.org/10.1016/j.egyr.2020.02.004.

[14] European Committee for Electrotechnical Standardization. Requirements for generating plants to be connected in parallel with distribution networks – Part 1: Connection to a LV distribution network. EN 50549-1:2019. CENELEC, Brussels, 2019.

[15] International Electrotechnical Commission. Wind energy generation systems – Part 12-1: Power performance measurements of electricity producing wind turbines. IEC 61400-12-1:2017. IEC, Geneva, 2017.

[16] Reda I, Andreas A. Solar Position Algorithm for Solar Radiation Applications. NREL Technical Report NREL/TP-560-34302. Golden, CO: National Renewable Energy Laboratory, 2008.

[17] Dufresne A. Nanocellulose: From Nature to High Performance Tailored Materials. 2nd ed. Walter de Gruyter GmbH, Berlin, 2017.

[18] Kraichok A, Pacaphol K, Suvarnakich K. Upcycling Recovered Paper into Microcrystalline Cellulose and Nanocellulose: A Focus on Office Waste Paper and Old Corrugated Containers. Waste and Biomass Valorization. 2026;17:2671–2689. https://doi.org/10.1007/s12649-025-03268-2.

[19] Szafraniec M, Grabias-Blicharz E, Barnat-Hunek D, Landis EN. A Critical Review on Modification Methods of Cement Composites with Nanocellulose and Reaction Conditions during Nanocellulose Production. Materials. 2022;15(21):7706. https://doi.org/10.3390/ma15217706.

[20] Baral A, Kerjee NR, Jashi NA, Emon MIH, Basak M, Rahman MM, et al. Recovery of cellulose nanocrystal from mixed office wastepaper and the development of bio-based coating matrixes with enhanced water, gas, oil, and grease resistances for packaging. RSC Advances. 2025;15(17):13188–13198. https://doi.org/10.1039/d5ra01516b.

https://doi.org/10.14669/AM/224717

[21] International Organization for Standardization. Road vehicles — Test contaminants for filter evaluation — Part 1: Arizona test dust. ISO 12103-1:2016. ISO, Geneva, 2016.

[22] Menter FR. Two-equation eddy-viscosity turbulence models for engineering applications. AIAA Journal. 1994;32(8):1598–1605. https://doi.org/10.2514/3.12149.

[23] ANSYS Inc. Ansys Fluent Theory Guide. Release 2026 R1. ANSYS Inc., Canonsburg (PA), 2026. https://ansyshelp.ansys.com/public/Views/Secured/corp/v261/en/pdf/Ansys_Fluent_Theory_Guide.pdf (accessed 2026 Feb 06).

[24] U.S. Environmental Protection Agency. Emission Factors for Greenhouse Gas Inventories (GHG Emission Factors Hub). DC: US EPA, Washington, 2025.

[25] Babamohammadi S, Birss AR, Pouran H, Pandhal J, Borhani TN. Emission control and carbon capture from diesel generators and engines: a decade-long perspective. Carbon Capture Science & Technology. 2025;14:100379. https://doi.org/10.1016/j.ccst.2025.100379.